*Int. J. Electrochem. Sci.*, 15 **(2020)** 4218 – 4231, doi: 10.20964/2020.05.02

International Journal of
ELECTROCHEMICAL
SCIENCE
www.electrochemsci.org

# Catalytic Activity of Strontium Modified $TiO_2$ Nanotubes for Hydrogen Evolution Reaction

*Khadijah M. Emran*

Chemistry Department, College of Science, Taibah University, Al-Madinah Al-Monawarah, Saudi Arabia.
E-mail: kabdalsamad@taibahu.edcu.sa

*Received:* 11 November 2019 / *Accepted:* 15 February 2020 / *Published:* 10 April 2020

A highly active electrochemical catalyst consisting of a strontium/titanium dioxide nanotubes (Sr-TNTs) composite was developed for the hydrogen evolution reaction (HER). The TNTs and Sr-TNTs were synthesized by direct hydrothermal synthesis. The morphology of the final product was characterized by SEM, EDX, X-ray diffraction (XRD) and Raman spectroscopy. The enriched Sr-TNT/Pd modified catalyst on Au electrode with highly dispersed nanoparticles and uniform Sr nanocrystallites provides an efficient electrocatalyst, leading to a superior HER activity with lower activation energy (5.56 kJ/mol) and optimum current density (1.393 $mA/cm^2$) compared to undoped TNT/Pd in 0.1 mol $L^{-1}$ $H_2SO_4$ solution. The reaction is determined to follow the Volmer–Tafel mechanism. The exceptional performance of the Sr-TNT/Pd cathodes is due to the unique semiconducting properties of the Sr-TNTs structure, which provide abundant Pd active sites with optimized atomic hydrogen binding energies in acidic media for the hydrogen production. A mechanism for the HER on Sr-TNTs/ Pd has been proposed where both the hybrid metal (Sr) and the support metal (Pd) are involved in the charge transfer process.

**Keywords:** Electrocatalysts; Strontium-$TiO_2$ nanotubes; Hydrothermal; Hydrogen generation; Activation energy.

## 1. INTRODUCTION

The production of hydrogen plays an important role in energy conversion and the development of hydrogen-based energy sources. Hydrogen generation is of great technological importance due to the increasing need to store renewable energy as hydrogen gas. Although extensive research has been carried out in the past 10 years on producing hydrogen fuel, the sustainable production of hydrogen remains a challenge [1-3]. Sustainable production requires low-cost catalysts, pollution-free sources for generating hydrogen and efficient conversion into useful energy. Hence, it is imperative to expand the current hydrogen production capacity using stable catalysts to meet the increasing hydrogen demand. Generally,

an effective approach to improving the activities of catalysts is to expose more catalytically active sites by increasing the electrochemical surface area [4]. According to this principle, nanomaterials are excellent candidates for high-surface-area catalysts [5]. Among the available nanotube materials systems, $TiO_2$ nanotubes (TNTs) are one of the most favorable nanomaterials for research. The unique characteristics of $TiO_2$ nanotubes, including large surface area, high aspect ratio and pore volume, chemical stability and environmental friendliness, have resulted in TNTs being widely explored for various applications [6-9]. However, the widespread application of TNTs is still limited because of their high band-gap energy of approximately 3.2 eV for anatase $TiO_2$. The electrolytic and/or photolytic activities of $TiO_2$ nanotubes can be improved by doping with metals [10-14 ] or nonmetals [ 15-17]. Su *et al.* [18] enhanced the photocatalytic activity of $TiO_2$ nanotubes for efficient hydrogen evolution by developing versatile multijunction photocatalysts composed of $SrTiO_3/TiO_2$ nanotubes, N-doped $TiO_2$, and platinum (Pt) as the internal, middle, and outer layer materials, respectively. Dubey *et al.* [19] modified $TiO_2$ nanotube arrays (TNTAs) with $Cu_2O$ nanoparticles to enhance the photoelectrochemical properties and hydrogen generation efficiency of TNTAs. Similarly, Lačnjevac *et al.* [20] deposited Pd nanoparticles on the walls of TNTAs for cost-effective hydrogen evolution. Recently, Zhao *et al.* [21] studied the synergistic effects between $TiO_2$ nanosheets and two different sizes of Au nanoparticles for efficient photocatalytic hydrogen evolution. Emran and Alanazi confirmed the excellent performance of Nd-Gd-Pt-TNTAs in hydrogen evolution with a very small activation energy ($E_a$) in acidic media [22].

Additionally, because driving the hydrogen evolution reaction (HER) demands significant energy, a considerable overpotential is required to overcome the large energy barrier. The usage of nano materials as electrocatalysts could reduce the reaction barrier significantly and enable efficient water splitting. In other words, an advanced electrocatalyst with high catalytic activity for HER should exhibit low overpotential, low activation energy and low Tafel slope for clean hydrogen fuel production [9]. Herein, we distributed Sr nanoparticles in $TiO_2$ nanotubes and demonstrated enhanced water-splitting hydrogen evolution reaction (HER) in acidic media. The $TiO_2$ nanotubes (TNTs) and doped Sr-TNTs were synthesized by a hydrothermal method. The as-prepared samples were compared with TNT/Pd and Sr-TNT/Pd to show the enhancement caused by Pd electrodeposited as support metal on the catalysts in 0.1 mol $L^{-1}$ $H_2SO_4$ solution. Kinetic and thermodynamic studies were carried out in order to determine the activation energy and the reaction mechanis Additionally, because driving the hydrogen evolution reaction (HER) demands significant energy, a considerable overpotential is required to overcome the large energy barrier. The usage of nanomaterials as electrocatalysts could significantly reduce the reaction barrier and enable efficient water splitting. In other words, an advanced electrocatalyst with high catalytic activity for HER should exhibit low overpotential, low activation energy and low Tafel slope for clean hydrogen fuel production [9]. Herein, we distributed Sr nanoparticles in $TiO_2$ nanotubes and demonstrated an enhanced water-splitting hydrogen evolution reaction (HER) in acidic media. $TiO_2$ nanotubes (TNTs) and doped Sr-TNTs were synthesized by a hydrothermal method. The as-prepared samples were compared with TNT/Pd and Sr-TNT/Pd to show the enhancement caused by Pd electrodeposited as a support metal on the catalysts in 0.1 mol $L^{-1}$ $H_2SO_4$ solution. Kinetic and thermodynamic studies were carried out to determine the activation energy and the reaction mechanism.

## 2. EXPERIMENTAL SECTION

### *2.1. Preparation of TNTs and Sr-TNTs*

An alkaline hydrothermal treatment was utilized to prepare titanium dioxide nanotubes, TNTs. The nanoparticles were developed into titanate sheets before being rolled into nanotubes. Approximately 0.5 g of P25 $TiO_2$ powder (P25, 99.5 %, 21 nm, Sigma-Aldrich, USA) was dispersed in sodium hydroxide solution (10 mol $L^{-1}$ NaOH, Sigma-Aldrich, USA) and sonicated for 30 min. The resulting alkaline solution was transferred to a 100 mL stainless steel autoclave container, which was tightly sealed and heated for 24 h at 150 °C. Then, the mixture was filtered and repeatedly washed with deionized water (Milli-Q® CLX 7000 Series, Millipore) and diluted HCl (HCl, Sigma-Aldrich, USA) until the solution reached a pH of 6. Finally, the white powder-form TNTs was dried for 10 h at 90 °C and calcinated at 400 °C for 2 h. The catalytic activity of the TNTs was improved using an in situ doping strategy to create Sr-TNTs. A 20:5 molar ratio mixture of titanium oxide and strontium nitrate $TiO_2$:$Sr(NO_3)_2$ ($Sr(NO_3)_2$, Sigma-Aldrich, USA) was dispersed in sodium hydroxide solution in the first step. Then, the hydrothermal treatments in autoclave container at 150 °C and postsynthetic treatments (washing by DI and HCl , draying and calcinate) were carried out in the same way as the synthesis of the undoped TNT.

### *2.2. Characterization of The Nanotubes*

The detailed surface structure and morphology of the TNTs and Sr-TNTs were characterized using scanning electron microscopy (SEM, Superscan SS-550, Shimadzu, Japan). The crystalline phases were identified and the elemental composition of the samples was analyzed by X-ray diffraction (XRD, Shimadzu, XRD-7000, Japan) at a scanning rate of 2°/min from $2\theta = 20°$ to 80° at 40 kV and 30 mA using a $CuK_\alpha$ incident beam ($\lambda$=0.154 nm) and energy dispersive X-ray analysis (EDX, Superscan SS-550, Shimadzu, Japan). The surface area of the TNTs and Sr-TNTs was measured by a Brunauer-Emmett-Teller (BET) analysis on a Micromeritics analyzer (Gemini VII, 2390 Surface Area and Porosity USA). Raman spectra were collected using a Raman microscope (Raman, Sentrarra, Bruker, USA) coupled to a Leica microscope (Olympus BX series, USA) using 532 nm excitation radiation.

### *2.3. Experimental Procedures*

Cyclic voltammetry (CV), electrochemical impedance spectroscopy (EIS), and linear polarization measurements were performed in 0.1 mol $L^{-1}$ $H_2SO_4$ solution (Sigma-Aldrich, USA) using an electrochemical analysis system based on a potentiostat/galvanostat (Gamry interface 1000 potentiostat) coupled with a personal computer. A gold (Au) electrode modified with TNTs or Sr-TNTs ($A$ =0.07 $cm^2$), an Ag|AgCl|KClsat electrode and a platinum wire were used as the working, reference and measurement electrodes, respectively. Assuming a linear relationship $log\ |i_o| = f\ (T^{-1})$ and using the Arrhenius equation, the apparent activation energy was determined. To control the cell temperature, the electrochemical cell was connected to a thermal bath, which allowed water to circulate around the cell. To prepare the electrochemical catalyst, a Au electrode was polished to mirror smoothness with slurry,

rinsed with DI water and dried in air. Then 6 µL of TNTs or hybrid-nanostructure Sr-TNTs were dropped onto the Au electrode and dried. Thus, a uniform film of modified electrode (Au/ TNT or Sr-TNT) was obtained. Then, Pd, which acts as a support catalyst, was deposited from a 0.001 M $PdCl_2$/0.1 M HCl solution by applying a double potential step (0 V for 30 s then 0.1 V for 10 min) to produce a (Au/TNT or Sr-TNT/Pd) electrode. For Au/Pd electrode, double potential step method was used to produce a uniform Pd layer on Au electrode.

## 3. RESULT AND DISCUSSION

### *3.1 Sample Characterization*

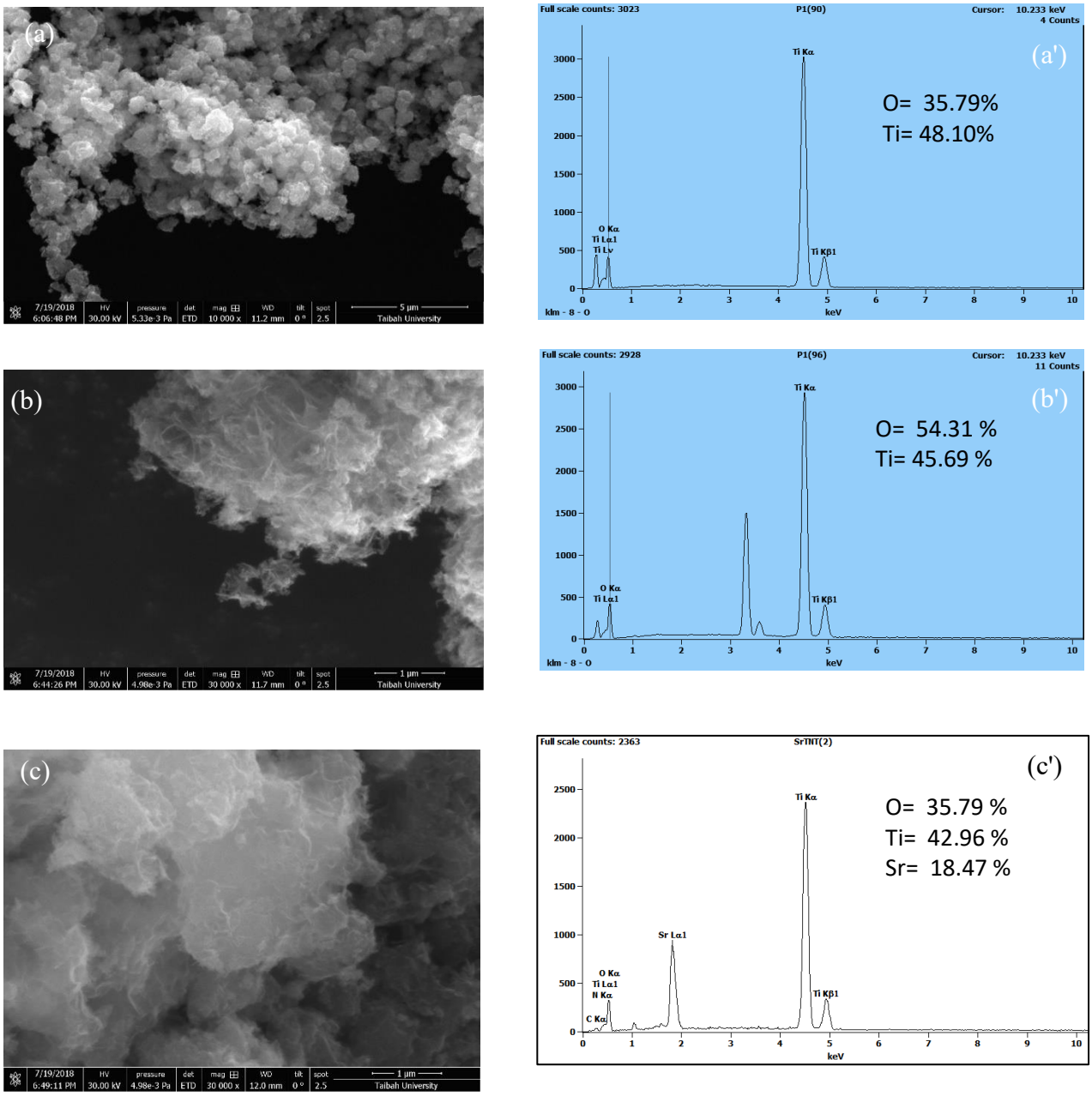


**Figure 1.** SEM and EDX images of (a,a') P25 $TiO_2$; (b,b')TNT and (c,c') Sr-TNT.

Scanning electron microscope photographs (Fig. 1a) show that the P25 $TiO_2$ particles took the form of highly aggregated spherical particles.

The TNTs and Sr-TNTs were made up of nanotubes interwoven together in a network (Fig. 1b, c). The cylindrical shape of the nanotubes was confirmed by the tubular structure of the synthesized samples. To confirm the existence of Sr nanoparticles, the approximate compositions of P25, the TNTs and the doped Sr-TNTs were measured by energy-dispersive X-ray spectroscopy (EDX, Fig. 1a', b' and c').

Elemental abundances of 18.47 wt% Sr, 42.96 wt% Ti, and 35.79 wt% O were observed in the Sr-TNTs catalyst. The XRD patterns of the P25 $TiO_2$, TNTs and Sr-TNTs exhibited diffraction peaks at $2\theta = 25.3°$, 37.8°, 48.0° and 55.1° corresponding to the (1 0 1), (0 0 4), (2 0 0) and (2 1 1) crystallographic planes, respectively. The patterns were similar to XRD patterns observed in the literature [23-25], which suggests a crystalline TNT structure in the tubes composed of the anatase $TiO_2$ phase (Joint Committee on Powder Diffraction JCPDS no. 21-1272). The other diffraction peaks at 31.9° and 32.6° and 46.7° corresponded to the (1 0 7), (1 1 0) and (2 0 0) crystallographic planes of $Sr_4Ti_3O_{10}$ (JCPDS no. 22-1444).

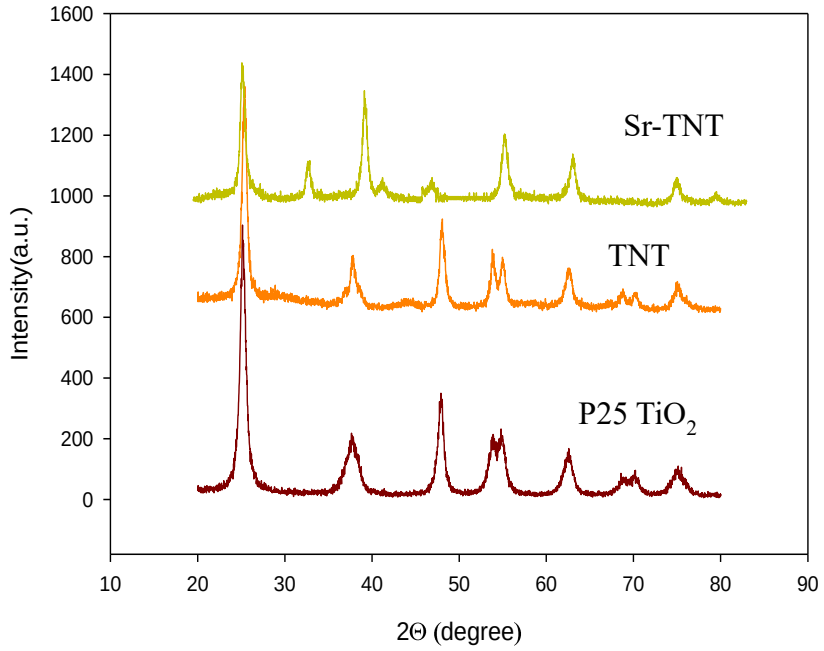


**Figure 2.** XRD patterns of P25 $TiO_2$, TNT and Sr-TNT calcined at 400 °C for 2 h.

Scherrer's equation (Eq. 1) was used to calculate the average particle size of the Sr doped in the TNT lattice, where D is the average particle size (nm), K is the shape-sensitive coefficient (0.9), λ is the wavelength of radiation used (1.540 nm), β is the full-width half-maximum of the Sr (1 0 7) peak (in rad), and θ is the angle at the position of the peak maximum (in rad)[26]:

$$D = \frac{K\lambda}{\beta \cos\theta} \quad (1)$$

It is apparent from the XRD data in Table 1 that the Sr nanoparticles in the additively treated $TiO_2$ sample were smaller and the surface area was higher than those of the undoped TNT samples. The slight reduction of the $TiO_2$ crystal volume after Sr modification suggests that Sr nanoparticles were located inside the $TiO_2$ unit cells at the grain boundary, thus hindering grain growth [27].

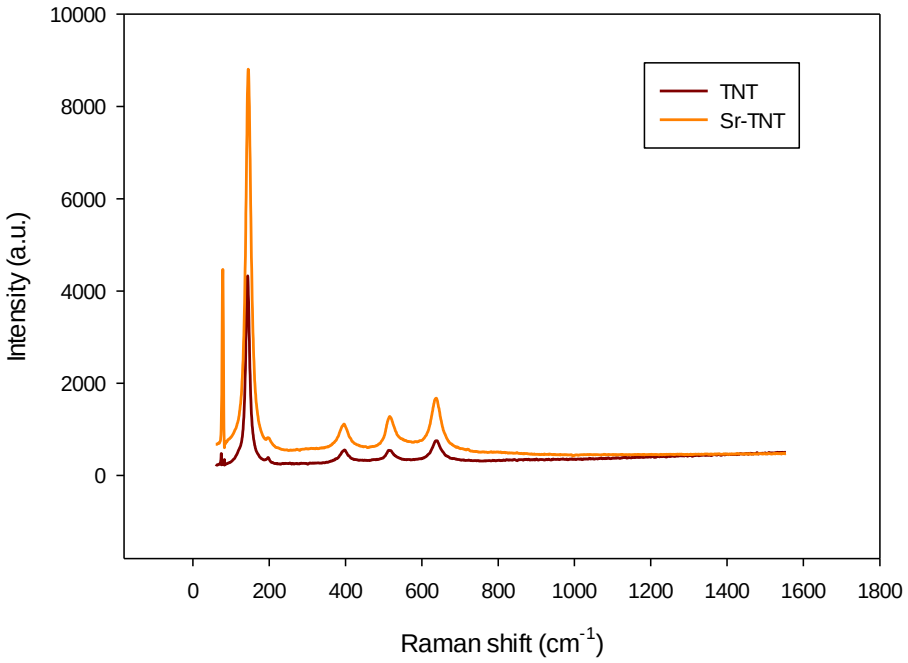


**Figure 3.** Raman spectra of the undoped TNT and doped Sr-TNTs calcined at 400 °C for 2 h.

**Table 1.** Average particle size from XRD data and BET surface area, pore volume and pore size of synthesis TNTs samples.

| Sample | Average Particle Size (nm) | BET Specific Surface Area, $S_{BET}$($m^2$/g) | Pore Volume ($cm^3$ $g^{-1}$) | Pore Size (°A) |
|---|---|---|---|---|
| **P25 $TiO_2$** | 7.31 | 58.90 | 0.047 | 16.9 |
| **Undoped TNTs** | 7.08 | 120.64 | 0.048 | 16.05 |
| **Sr-TNTs** | 6.96 | 174.941 | 0.052 | 16.07 |

Moreover, the textures of the synthesized nanotubes were determined using BET theory and are listed in Table 1. The BET surface area of the modified Sr-TNTs was 175 $m^2$ $g^{-1}$, which was approximately 3 times larger than the P25 surface area and 0.7 times larger than the surface area of

undoped TNTs. The micropore volume and pore size of the doped Sr-TNTs were 0.052 $cm^3$ $g^{-1}$ and 16.07 Å, respectively, suggesting that they included a considerable micropore volume in their framework, which can be attributed to enhanced mesoporosity [28].

Fig. 3 shows the Raman spectra of the undoped and doped TNTs. According to the three symmetry group analysis modes (A1g; 2B1g; 3Eg), the anatase-phase TNTs and Sr-TNTs had some Raman active peaks that appeared at 144.1 ($E_g$), 199.8 ($E_g$), 397.8 ($B1_g$), 515.1 (B1g), and 638.5 $cm^{-1}$ [20-29-31].

### *3.2 Catalytic Activity Toward HER*

The electrochemical and catalytic performance of TNTs and doped Sr-TNTs for HER were investigated by linear polarization and cyclic voltammetry. The cyclic voltammetry responses of bare Au, Au/TNTs, Au/TNTs/Pd, Au/Sr-TNTs and Au/Sr-TNTs/Pd electrodes in 0.1 mol $L^{-1}$ $H_2SO_4$ solution at a scan rate of 100 $mVs^{-1}$ are shown in Fig. 4a. As displayed in Fig. 4a, and Table 2, Au/Sr-TNTs/Pd demonstrated the highest HER activity of all the electrodes in acidic media and required an overpotential of just 149 mV with a maximum reduction current of 1.49 mA $cm^{-2}$. The Au/Sr-TNTs exhibited an acceptable overpotential of 165 mV to drive 1.19 $mAcm^{-2}$ in 1.0 mol $L^{-1}$ $H_2SO_4$, which was relatively low compared to that of Au/TNTs/Pd (210 mV to drive 1.30 $mAcm^{-2}$). Comparing these results to the overpotential of 206 mV required to drive 0.89 $mAcm^{-2}$ in the undoped Au/TNTs clearly confirms the importance of dopant and support metals to enhancing catalyst activity. As expected, no such response was observed for the bare Au electrode because of the absence of a catalyst.

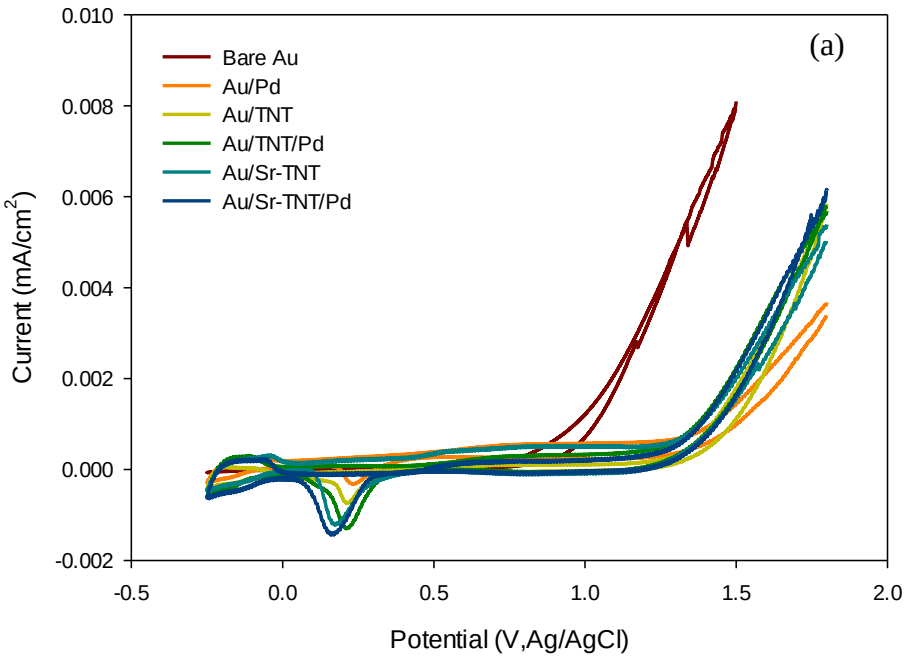

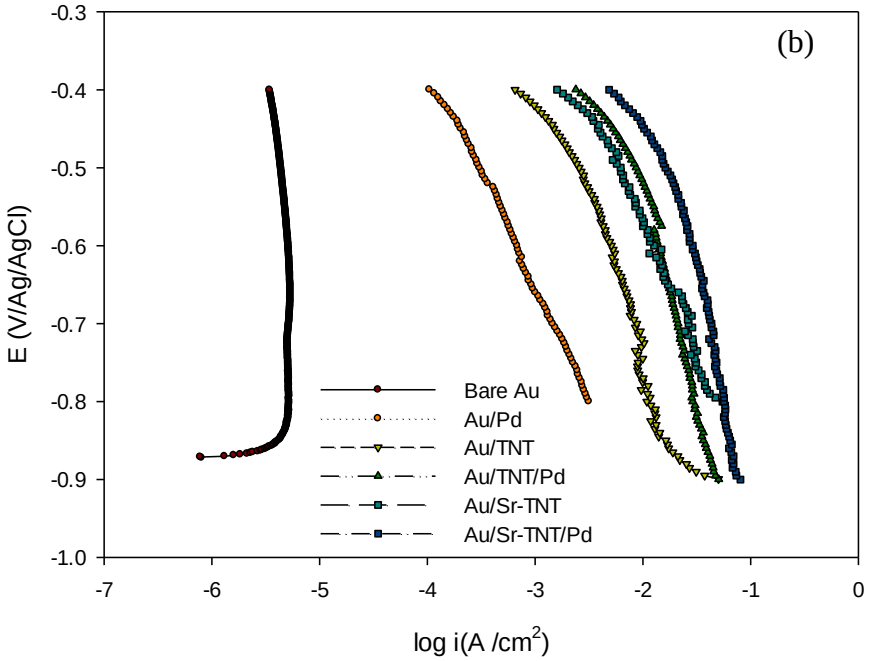


**Figure 4.** (a) Cyclic voltammetry responses and (b) linear Tafel polarization curves for HER on bare Au, Au/Pd, Au/TNT, Au/TNT/Pd, Au/Sr-TNT and Au/Sr-TNT/Pd in 0.1 mol $L^{-1}$ $H_2SO_4$.

**Table 2.** Summary of the catalytic activity of the TNTs electrocatalysts in 0.1 mol $L^{-1}$ $H_2SO_4$.

| | **Cyclic Voltammetry** | | **Linear Tafel Polarization** | | |
|---|---|---|---|---|---|
| **Catalyst Type** | I ($mA/cm^2$) | -E(mV) | -b (mV/dec) | $-j_o$ ($\mu A/cm^2$) | $-j$ ($\mu A/cm^2$) at -400 mV |
| **Bare Au** | - | - | 843 | 2.1 | 3.5 |
| **Au/Pd** | 0.306 | 230 | 285 | 5.24 | 102 |
| **Au/TNTs** | 0.89 | 206 | 255 | 84.5 | 679 |
| **Au/TNTs/Pd** | 1.30 | 210 | 246 | 551.9 | 1540 |
| **Au/Sr-TNTs** | 1.19 | 165 | 231 | 1198.97 | 2402 |
| **Au/Sr-TNTs/Pd** | 1.49 | 149 | 216 | 1205.09 | 4920 |

The same trend of HER electrocatalytic activity was observed in the Tafel linear polarization measurements. Fig.4b shows a set of Tafel curves recorded in 0.1 mol $L^{-1}$ $H_2SO_4$ in the potential region of hydrogen evolution for Au electrodes modified with catalysts. The Tafel plots of the catalysts were created by fitting their corresponding polarization curves with the Tafel equation ($\eta = a + b \log (-j_o)$), where $\eta$ is the overpotential, b is the Tafel slope and $j_o$ is the current density. By considering the active region (the Tafel region), the values of the Tafel slope and exchange current density calculated for the prepared catalysts were determined and are listed in Table 2. The Au/Sr-TNTs/Pd-modified electrode

showed the best electrochemical performance for HER, with a cathodic current of approximately 1205 μA/cm$^2$ and a Tafel slope of 216 mV/dec.

The exchange current density is a well-known parameter for the characterization of electrocatalytic activity [32]. To evaluate the electrocatalytic activity of the TNTs prepared in this study for use in hydrogen generation, we fixed the overpotential (i.e., hydrogen production power) and measured the resulting current density (i.e., hydrogen production rate). The measured current densities *j* (μA/cm$^2$) at -400 mV are presented in Table 2. Again, the Sr-TNTs/Pd-modified electrode provided the highest hydrogen production rate and followed a trend similar to that of the exchange current density. The shape of the Tafel curves in Fig. 4b suggests a diffusion-limited reaction controlled by mass transport through the narrow pores in the tubular structures of the catalysts [33,34].

There are two possible reaction mechanisms for the HER in acidic media [35]. The first step in both mechanisms is the Volmer reaction, where $H_3O^+$ adsorption takes place after an electron transfer on the surface of the electrodes:

$$M + H_3O^+ + e \rightarrow M - H_{ads} + H_2O \quad (b=2.303RT/\alpha F\approx 120 \text{ mV/ dec}) \quad (2)$$

The next step is followed by either a Heyrovsky reaction (Volmer–Heyrovsky mechanism)

$$M - H_{ads} + H_3O^+ + e \rightarrow H_2 + M + H_2O \ (b = 2.303RT/(1+\alpha)F\approx 40 \text{ mV/dec}) \quad (3)$$

or by a Tafel reaction involving the chemical recombination of two $H_{ads}$ atoms (Volmer–Tafel mechanism):

$$M - H_{ads} + M - H_{ads} \rightarrow H_2 + 2M \quad (b=2.303RT/(1+\alpha)F\approx 30 \text{ mV/dec}) \quad (4)$$

For the value of *b* given in each reaction, R is the ideal gas constant, T is the absolute temperature, α = 0.5 is the symmetry coefficient, and F is the Faraday constant. The Tafel slope is an intrinsic property of the catalysts, which can be used to evaluate their catalytic activity and is determined by the rate limiting step of the HER [36,37]. The Tafel slope for the Sr-TNTs/Pd catalyst samples was 216 mV.dec$^{-1}$. This was replicated for all of the catalysts studied, suggesting that the HER followed the Volmer-Tafel mechanism and that Sr-TNTs/Pd and the other catalysts were influenced by both electron transfer and hydrogen adsorption. This outcome confirms that the Pd nanoparticles were only used as support catalysts and enhanced the conductivity with a lower onset overpotential of the nanotubes. The electron transfer within the modified materials was facilitated by the Sr-TNTs, which enhanced the catalytic activity [18].

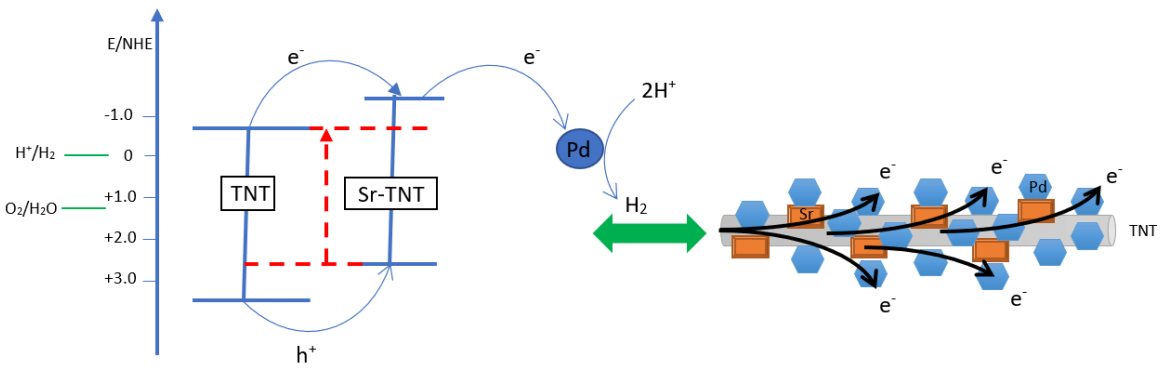


**Figure 5.** Mechanism of electrocatalysts and hydrogen reduction on Au/Sr-TNT/Pd.

As shown in Fig. 5, the $TiO_2$ nanotubes exhibited better electron transport ability because of the direct conduction pathway provided by the $TiO_2$ nanotubes. The doped Sr nanoparticles created mid-band-gap levels between the conduction band and valance band [18]. Specifically, small amounts of metal dopants such as Sr can act as electron sinks to generate more electron-hole pairs [20], which improves electronic delivery and enhances charge transfer, while Pd provides weak $H_{ads}$ binding energies in acidic media [20,38]. This could explain the synergistic effect between the Sr nanoparticles and support metals such as Pd on $TiO_2$ with regard to enhancing hydrogen evolution.

### *3.3 Electrode Resistance and Stability*

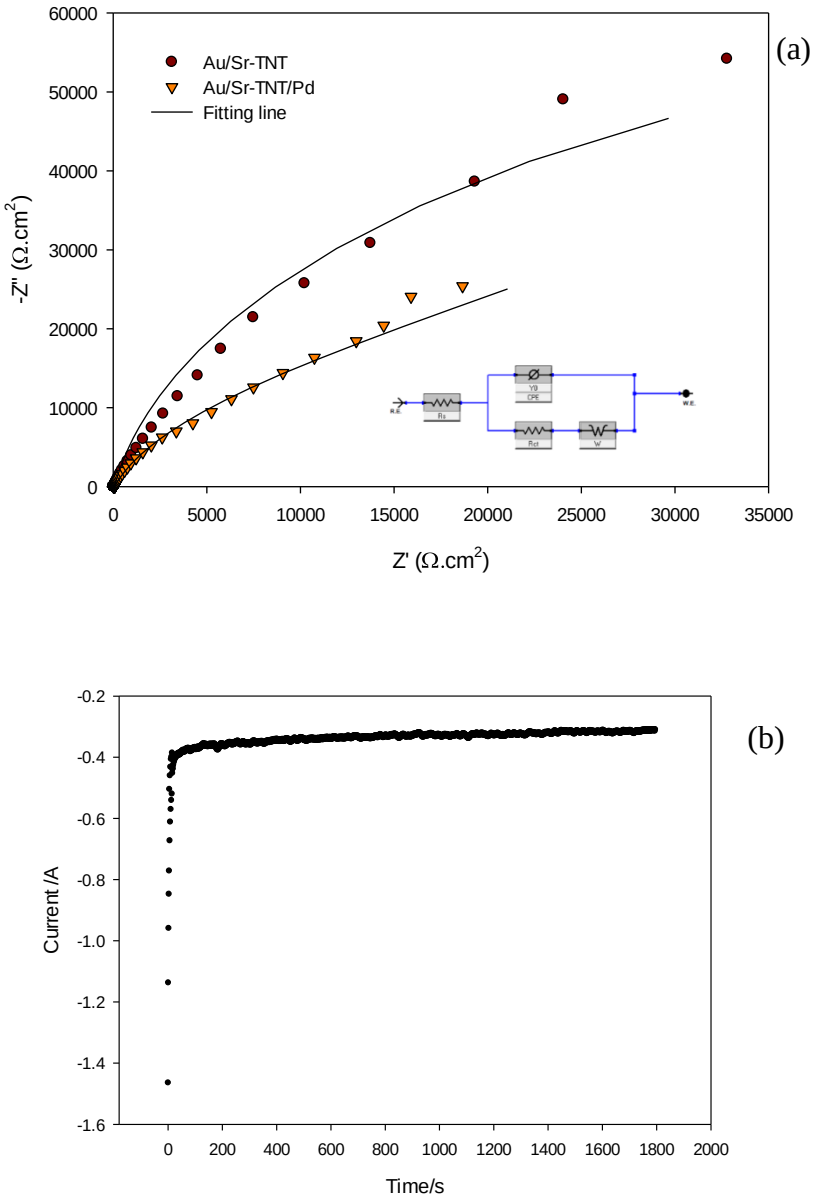


**Figure 6.** (a) Nyquist plots for Au/Sr-TNT/Pd at 150 mV and Au/Sr-TNT/Pd at -165 mV and the equivalent circuit to fit the EIS; (b) the stability of Sr-TNT/Pd catalyst by the potentiostatic experiment at 150 mV in 0.1 mol $L^{-1}$ $H_2SO_4$.

EIS is an important technology for studying the electrode kinetics of HER. The EIS of the Sr-TNTs layer was measured at -165 mV in 0.1 mol $L^{-1}$ $H_2SO_4$ solution and Fig. 6a displays a semicircle at high-to-medium frequencies for the charge transfer resistance with a diffusion controlled electrochemical processes at low frequencies. After modification of the Sr-TNTs catalyst with Pd, the $R_{ct}$ at -150 mV decreased. It can be seen that behavior similar to diffusion is exhibited. The impedance data were fitted using an equivalent circuit (inset of Fig. 6a). One semicircle was evidence of an electrode/electrolyte double layer capacitance in the equivalent circuit. This is consistent with the absence of a Pd partial layer on the TNT surface. In the equivalent circuit, $R_s$ is the resistance of the acid electrolyte; *CPE* and $R_{ct}$ are the phase constancy element and the charge transfer resistance, corresponding to the semicircle; and *W* is the Warburg impedance engendered from the semi-infinite diffusion of $H^+$ in the electrode, which is generally indicated by a sloping tail at low frequencies.

The value of charge transfer resistance ($R_{ct}$) is obtained. The value of $R_{ct}$ is usually used to characterize the electrocatalytic activity of a catalyst. The lower value of $R_{ct}$ indicates the high catalytic activity for catalyst [39,40].

The decreased value of $R_{ct}$ from 64 KΩ.$cm^2$ for TNT to 52 KΩ.$cm^2$ for Sr-TNT catalyst indicates that Pd had been successfully connected to the electrode surface accelerating the electron transfer. Similar behavior was detected for doped Ag/TNT [41], C-F/TNT [42] and Ni-N/TNT [43] for enhancing photocatalytic and/or electrical conductivity of $TiO_2$ induced by doping elements.

The long-term stability of electrocatalysts is also an important factor when judging the HER performance of a catalyst. During the 1800 s continuous test at 150 mV, the current increased sharply for the first 18 s and then stabilized, as depicted in Fig. 6b. There was a slight current shift (less than 5.13 mA) for the Sr-TNTs/Pd catalyst. This indicates that the Sr-TNTs/Pd catalyst exhibited better durability, stability and very low rate of surface poisoning under acidic conditions [44,45].

### *3.4 Activation Energy*

To determine the effect of temperature on the kinetic parameters of the HER, Tafel plots were recorded for the TNTs with and without Sr doping at different temperatures. The Tafel plots provided measurements of the exchange current density, $i_o$, and the activation energy, $E_a$ [37]. The exchange currents, $i_o$, were taken from the intersection of the Tafel slope with the abscissa (*log* $|i_o|$)[46]. Fig.7 displays the DC linear polarization (Tafel) measurements of Au/TNT/Pd and Au/Sr-TNT/Pd catalysts for temperatures ranging from 303 K to 333 K. The values (ca. ≈520 mV/dec to ≈560 mV/dec) of the Tafel slopes for HER on both Au/TNT/Pd and Au/Sr-TNT/Pd electrodes indicate that the rate-determining step was the transfer of the first electron in both solutions and the rate-limiting step did not change with temperature [20, 22,47]. These were similar to that previously observed by Galal et al.[48] for $SrPdO_3$ perovskite catalyst (Tafel slope = 871.4 mV/dec) prepared by the citrate method and used as electrocatalyst for HER in 0.1 mol $L^{-1}$ $H_2SO_4$ solution. Recently Emran and A. Alsahli [49] had determined the Tafel slope of TNT/Pt+Pd about ≈196 mV/dec and for Sn-TNT/Pt+Pd about ≈215 mV/dec for HER in 0.1 mol $L^{-1}$ $H_2SO_4$ solution. These data suggested that HER on TNTs catalysts is follows the Volmer-Tafel mechanism, where the rate of first electron include as determining step with hydrogen adsorption step.

The exchange current densities for the HER with the Au/Sr-TNT/Pd catalyst examined in this study were on the order of A/cm$^2$ and were higher than those at the Au/TNT/Pd electrode surface. This higher exchange current density may indicate that active sites at the Sr-TNT/Pd catalyst surface were much more active than the terrace sites for the HER.

A temperature increase, i.e., enhancement of the thermal motion, leads to an increase in the distance up to which $H_3O^+$ may approach the catalyst surface and a corresponding exchange current increase. Figs. 7a' and 7b' demonstrate that the exchange current followed the Arrhenius equation using a semilogarithmic plot [50]:

$$\log i_o = -E_a/2.303RT + \log A \quad (5)$$

where A (A.cm$^{-2}$) is the pre-exponential factor, and $E_a$ (J.mol$^{-1}$) is the apparent activation energy. Thus, from the slope of the line, the apparent activation energy value can be calculated. The activation energy values for TNT/Pd and Sr-TNT/Pd catalysts were 9.23 and 5.56 kJ.mol$^{-1}$, respectively. The $E_a$ of free TNT in this study is close to value of free TNTs Arrays catalyst (≈10.79 kJ.mol$^{-1}$)[22] and letter higher than TNT/Pt+Pd catalyst (≈ 8.75 kJ/mol)[49] for HER in 0.1 mol L$^{-1}$ $H_2SO_4$ solution. But it is very lower compare to $SrPdO_3$ perovskite catalyst (≈ 27.9 kJ/mol) in same solution.

The difference between the two $E_a$ values can be explained on the basis that the catalytic activity of Sr-TNT/Pd was higher than that of TNT/Pd, which was expected since Sr-TNT/Pd is a hybrid metal that creates a proton reductive dopant in the TNT lattice and modifies its electrocatalytic properties.

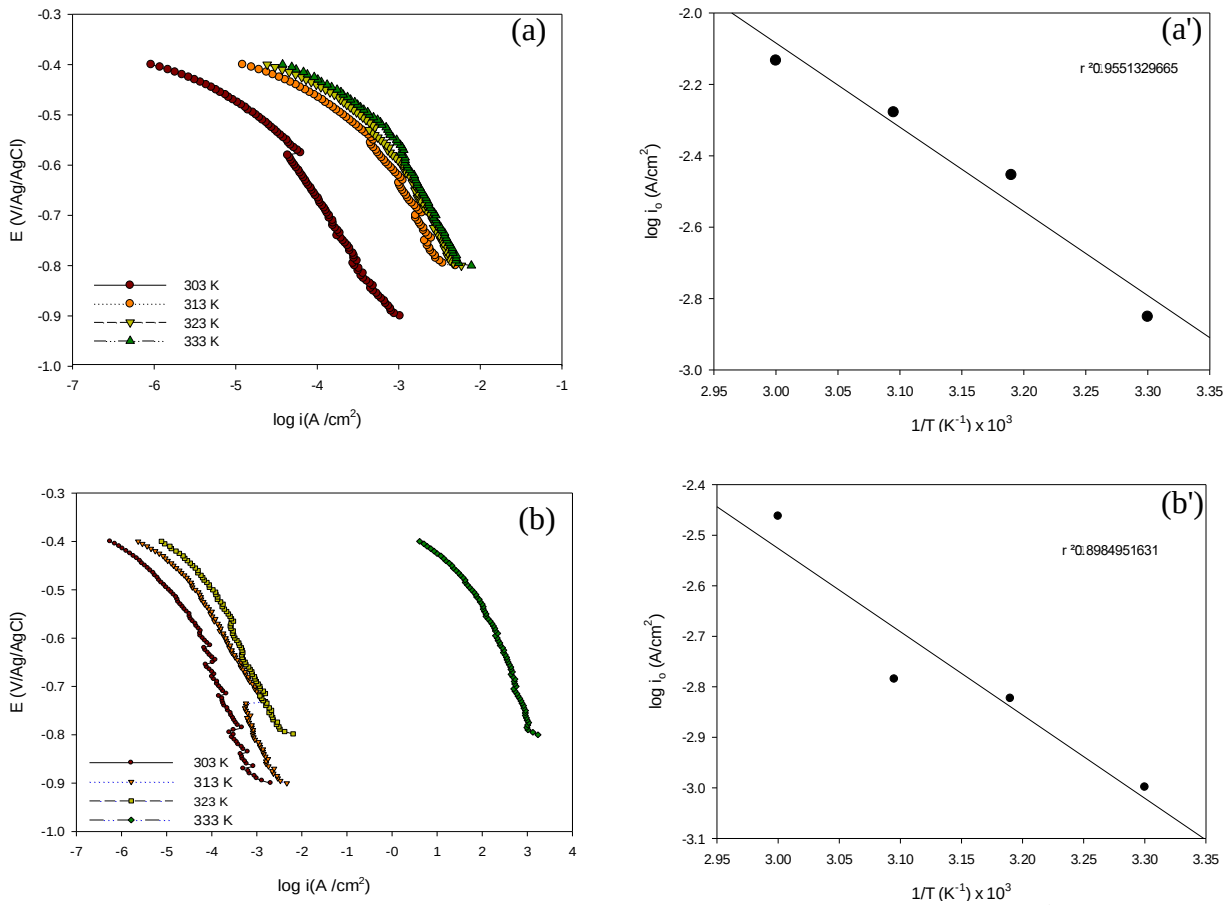


**Figure 7.** Tafel plots for HER at (a) Au/TNT/Pd and (b) Au/Sr-TNT/Pd in 0.1 mol L$^{-1}$ $H_2SO_4$. at various constant temperatures. Corresponding Arrhenius plots for HER at (a') Au/TNT/Pd and (b') Au/Sr-TNT/Pd.

## 4. CONCLUSION

TNT and Sr-TNTs catalysts in the anatase phase were successfully prepared by hydrothermal methods. The self-supported TNT/Pd and Sr-TNT/Pd composite electrodes exhibited excellent catalytic activity and HER kinetics in 0.1 mol $L^{-1}$ $H_2SO_4$ solution. The Sr-TNT/Pd surpassed the TNT and TNT/Pd catalysts in apparent HER activity. The outstanding HER performance of the Sr-TNT/Pd cathodes can be attributed to three factors. First, the three-dimensional TNT structures provide large surface areas. Second, the favorable utilization of a hybrid metal provides intermediate levels and increased electron-hole pairs to improve current flow. Finally, the effectiveness of the Pd catalytic sites reduces the atomic hydrogen binding energy, achieving highly efficient HER. The synthesis strategy presented in this study may open up new avenues for manufacturing TNT-supported, cost-effective electrocatalysts for HER and other cathodic reactions of practical importance in electrochemistry.

CONFLICT OF INTEREST

The authors declare that they have no conflicts of interest.

ACKNOWLEDGMENTS

The authors thank Prof. Abdullah Al-Mayouf from King Saud University for his helpful advice on various technical issues. In addition, the authors would like to thank technicians, Mr. Abdallah Jaber (physics department) and Miss. Fatemah Abdalraheem (chemistry department) for conducting surface measurements on the study samples.

## References

1. R. Chaubey, S. Sahu, O. James, S. Maity, *Renew. Sustain. Energy Rev.,* 23 (2013)443.
2. A. Eftekhari, *Int. J. Hydrogen Energy,* 42 (2017) 11053.
3. A. Lasia, *Int. J. Hydrogen Energy*, 44 (36)(2019) 19484.
4. B. Yu, F. Qi, Y. Chen, X. Wang, B. Zheng, W. Zhang, Y. Li, L.C. Zhang, *ACS Appl. Mater. Interfaces,* 36 (2017) 30703.
5. S. S.Mao, S.Shen, L.Guo, *Prog. Nat. Sct.-Matter.,* 22 (6)(2012) 522.
6. J .Huang, Y .Cao, Z .Deng, H .Tong *J. Solid State. Chem*., 184 (2011) 712.
7. K. Chen, K. Xie, X. Feng, S. Wang, R. Hu, H. Gu, Y.Li. *Int. J. Hydrogen Energy,* 37 (2012) 13602.
8. L. Clarizia, D. Russo, I. Di Somma, R. Andreozzi, R. Marotta, *Multifunctional Photocatalytic Materials for Energy,* Woodhead Publishing (2018) 187.
9. I.brahim, C.Athanasekou, G.Manolis, A. Kaltzoglou, N. K.Nasikas, F. Katsaros, E. Devlin, A. G.Kontos, P. Falaras, *J. Hazard. Mater.*, 372 (15) (2019) 37.
10. X. Chen, W. Liu, L. Tang, J. Wang, H. Pan, M. Du, *Mat. Sci. Eng.* C, 34 (2014) 304.
11. Z. Dong, D. Ding, T. Li, C. Ning, *Appl. Surf. Sci.,* 443 (2018) 321.
12. P. Parnicka, P. Mazierski, W. Lisowski, T. Klimczuk, J. Nadolna, A. Zaleska-Medynska, *Results Phys.,* 12 (2019) 412.
13. Y. Q. Wang, Z. D. Wei, B. Gao, X. Q. Qi, M. R. Xia*, J. Power Sources*, 196 (2011) 1132.
14. K.M. Emran, S. M. Ali, H. E. Alanazi, *J. Electroana. Chem.*, 856 (2020) 113661.
15. J. Zhang, Y. Wu, M. Xing, S.A.K. Leghari, S. Sajjad, *Energy Environ. Sci.,* 3 (2010) 715.
16. M. Abdullah, S. K. Kamarudin, L. K. Shyuan, *Nanoscale. Res. Lett.*, 11 (2016) 553.
17. D. Lu, M.Zhang, Z. Zhang, Q. Li, X. Wang, J. Yang *Nanoscale. Rer. Lett.,* 9 (2014)272.
18. E. Su , B. Huang , M. Wey, *Sol. Energy,* 134 (2016) 52.

19. P. K. Dubey, R. Kumar, R. S. Tiwari, O. N. Srivastava, A. C. Pandey , P. Singh, *Int. J. Hydrogen Energy,* 43 (2018) 6867.
20. U. Lačnjevac, R. Vasilićb, T. Tokarski, G. Cios, P. Żabiński, N. Elezović, N. Krstajić, *Nano Energy,* 47 (2018) 527.
21. Q. Zhao, Q. Zhang, C. Du, S. Sun, J. D. Steinkruger, C. Zhou, S. Yang, *Nanomaterials*, 9(4) ( 2019) 499.
22. K. M. Emran, H. E. Alanazi, *Fabrication and Growth Mechanism of Double Layer Lanthanide – Pt/$TiO_2$ Nanotube Arrays Electrode as a Cost- Highly Efficient Electrocatalyst for Hydrogen Evolution in Acid Media*, submited 2020.
23. W. Alves, A. O. Ribeiro, M. V. B. Pinheiro, K. Krambrock, F. El Haber, G. Froyer, O. Chauvet, R. A. Ando, F. L. Souza, and W. A. Alves, *J. Phy. Chem*. C, 115 (2011) 12082.
24. Y. Chai, L. Lin, K. Zhang, B. Zhao, D. He, *Ceram. Int.,* 40 (2014) 2691.
25. K. M. Emran, H. E. Alanazi, *Fabrication and Properties of Lanthanide-$TiO_2$ Nanotube Composites,* submited, 2020.
26. S. Huang, Z. Si, X. Li, J. Zou, Y. Yao, D. Weng, *Sens. Actuators B,* 234(2016) 264.
27. D. Kim, E.F. Abo Zeid, Y. Kim, *Electrochim. Acta*, 55 (2010) 3628.
28. M. Meksi, A. Turki, H. Kochkar, L. Bousselmi, C. Guillard, G. Berhault, *Appl. Catal. B,* 181 (2016) 651.
29. P. V. Viet, B. T. Phan, D. Mott, S. Maenosono, T. T. Sang, C. M. Thi, *J. Photochem. Photobiol. A,* 352 (2018) 106.
30. B. Tahir, M. Tahir, and N. A. S. Amin, *Energy Convers. Manage.,* 159 (2018) 284.
31. J.G. Highfield, K. Oguro, B. Grushko, *Electrochim. Acta,* 47 (2001) 465.
32. N. F. Atta, A.Galal, S. M. Ali, *Int. J. Electrochem. Sci.,* 9 **(2014)** 2132.
33. A. Galal, N.F. Atta, S. M. Ali, *Electrochim. Acta*, 56 (2011) 5722.
34. K. Yin, Y. Cheng, B. Jiang, F. Liao, M. Shao, *J. Colloid Interface Sci.,* 522 (2018) 242.
35. Z.Tang, L. Liao, Y.Zheng, J. Kang, Y. Chen, *Chin. J. Chem. Phys*., 25 (2012) 469.
36. J. Du, X. Wang, C. Li, X. Liu, L. Gu, H.Liang, *Electrochim. Acta*, 282 (2018) 853.
37. Y. Deng, C. Ye, G. Chen, B. Tao, H. Luo, N. Li, *J. Energ.Chem.*, 28 (2019) 95.
38. J. Durst, C. Simon, F.Hasch´e, H. A. Gasteiger, *J. Electrochem. Soc*., 162 (1) (2015) 190.
39. L.Z. Zhuang , L. Ge , Y.S. Yang , M.R. Li , Y. Jia , X.D Yao , Z.H. Zhu , *Adv. Mater.,* 29 (2017) 1606793.
40. S. M. Ali, K. M. Emran, H. A. Al lehaibi, *Int. J. Electrochem. Sci.,* 12 (2017) 8733.
41. D.Fang, K. Huang, S. Liu, Z. Li, *J.Alloy. Comp*., 464 (2008)L5.
42. H.Li, J.Xing, Z. Xia, J.Chen, *Electroch, Acta*, 139( 2014) 331.
43. D. Yan, C. Yu, X. Zhang, J. Li, J. Li, T. Lu, L. Pan, *Electrochim. Acta*, 254 (2017) 130.
44. A. Safavi , S. Momeni , M. Tohidi, *Electroanalysis*, 24 (2012) 1981.
45. M. Abdullah, S. K. Kamarudin, L. K. Shyuan, *Nanoscale Res. Lett.*, 11 (2016) 553.
46. M.R. Gennero de Chialvo , A.C. Chialvo, *J.Electroanal. Chem.*, 372 (1994) 209.
47. P. Xiao, M. A. Sk, L. Thia, X. Ge, R. J. Lim, J.Y. Wang, K. H. Lim, X. Wang, *Energy Environ. Sci.*, 7( 2014) 2624.
48. A. Galal, N.F. Atta, S.A. Darwish, A.Abdel Fatah, S.M. Alim, *J.Power Sources*,195 (2010) 3806.
49. K. M. Emran, R. M. A. Alsahli, "Efficient Hydrogen Production Electrocatalytic Using Hydrothermal Synthesized Sn-TNT", submited, 2020.
50. R. Cretu, A. Kellenberger, N. Vaszilcsin, Int. J. Hydrogen *Energy*, 38 (2013) 11685.

© 2020 The Authors. Published by ESG (www.electrochemsci.org). This article is an open access article distributed under the terms and conditions of the Creative Commons Attribution license (http://creativecommons.org/licenses/by/4.0/).